# Solar Exoskeletons – An integrated building system combining solar gain control with structural efficiency

Ramon Elias Weber*[a,b], Caitlin Mueller[a], Christoph Reinhart[b]

[a] Digital Structures Group, Department of Architecture and Urban Planning, Massachusetts Institute of Technology, 77 Massachusetts Avenue, Cambridge, MA 02139, USA, *reweber@mit.edu

[b] Sustainable Design Lab, Department of Architecture and Urban Planning, Massachusetts Institute of Technology

## 1. Abstract

We propose the use of solar exoskeletons, an integrated building system that combines material efficiency in structural load transfer with passive solar gain control. This offers an impactful way to respond to the UN climate goals, as the architecture and engineering disciplines face the challenge of delivering low carbon buildings. While the two goals of drastically reducing operational and embodied emissions are often considered independently, we can show how approaching them in tandem, through a novel building system, can offer significant savings. With large spans for maximum flexibility for residents and full glazing to maximize daylight, high-rise buildings are often suboptimal in terms of their material usage from steel frame construction and cooling demand from uncontrolled solar gains. We view solar exoskeletons as a sustainable pathway for future high-rise structures – combining solar gain control through external shading with a highly efficient structural system optimized for lateral loads in tall buildings. For this, we present an automated workflow that combines parametric modeling of architectural elements and structural simulation with Radiance-based annual radiation simulations and an operational energy model in EnergyPlus. Evaluating embodied carbon and energy use intensity of midrise and tower buildings in timber and steel, we compare hundreds of iterations for a prototypical building in Phoenix, USA. Our results show that exoskeletons can lead to embodied and operational carbon reductions in the lateral load-resisting structural system of 37-80% and 24-48%, respectively, vis-à-vis conventional construction techniques. Adding photovoltaic modules to the external shading system can lead to net zero building solutions for the buildings investigated in this case study.

## 2. Introduction

The built environment is one of the main contributors to climate change (Wörsdörfer et al. 2019). In the United States, building-related emissions account for 40% annual of carbon emissions (World Green Building Council (WGBC), IEA, and UN-Environment 2018). As the architecture and engineering disciplines face the enormous challenge of delivering carbon neutral buildings in the coming decades, it becomes clear that the required reductions of *both* embodied and operational energy of buildings will necessitate a rethinking of current design methodologies and building systems to position energy and carbon emissions as key design drivers (Ürge-Vorsatz et al. 2012). In architectural practice, building performance is largely determined during the early stages of architectural design (Aksamija 2015; Häkkinen et al. 2015), whereas thermal and structural assessments are still oftentimes conducted later in the design process when key decisions have already been made (Schlueter and Thesseling 2009; Schweber and Haroglu 2014). It seems vital that computational methods for both structural and thermal performance optimization and analysis are more closely integrated within early stages of design than currently available tools (Gao, Koch, and Wu 2019). We demonstrate how bridging the disciplinary divide between structural design and environmental performance can lead to more efficient architectural systems overall.

In the last decades, urban densification and economic growth have contributed to the proliferation of high-rise buildings, especially in hot climates across Asia, North America, and the Middle East (Taubenböck et al. 2020). These large-scale commercial developments are key elements of the global economy, offering spaces for enhanced productivity and commerce. The architectural intent to create productive indoor environments often results in the desire to build adaptable spaces (Arge 2005), as well as facades that maximize access to daylight and views. The resulting bias toward large spans of concrete and steel framing, along with substantial, uncontrolled heat gains through unshaded building envelopes (Assem and Al-Mumin 2010), stands in direct conflict with the optimal structural and energetic design needed to achieve buildings with low embodied and operational energy use.

Typical construction of multi-level office buildings involves a steel or concrete rectangular column grid, offset from the envelope in the interior space of a building, and a non-structural curtain wall façade (Schittich et al. 2013). When fully or mostly glazed, the façade becomes a primary source of unwanted solar heat gain with limited thermal benefits. As high windspeeds, climate conditions, and building codes make dynamic exterior shading louvers infeasible in tall buildings, passive fin systems, ornamental screens, or highly expensive multi-layer building envelopes are employed to prevent overheating (Herzog, Krippner, and Lang 2004). The resulting curtain wall façade and fin systems often involve highly carbon-intensive materials – such as steel and aluminum – that contribute to the overall embodied carbon, and add significant weight to a building (Lee et al. 2018). The key idea explored in this manuscript is to repurpose exterior façade and shading systems as "solar exoskeletons" that act as an exterior structure of a high-rise, reducing material use and allowing for more flexible floorplan layouts by eliminating interior structural columns besides a central circulation core. We are inspired by diagrid structural systems, that are used as structurally efficient systems for tall buildings (Moon, Connor, and Fernandez 2007; Liu et al. 2018). Diagrids play a similar role structurally but have not previously been optimized for thermal benefits, even though the resulting multifunctional system has structural and solar gain control functions. The interconnected grid of beam members on the exterior of the building is structurally efficient, especially with respect to counteract lateral loads (such as wind), as it is not restricted to a vertical column grid. Our analysis of the overall building system reveals multiple benefits from reducing material and operational energy use to more interesting architectural expressions. The investigated systems are visualized in Figure 1.

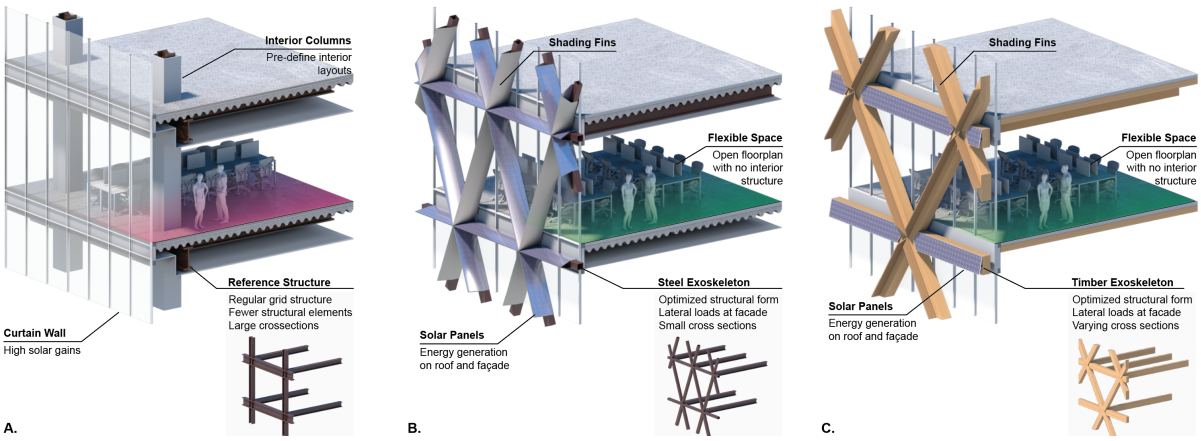


*Figure 1: Visualization of the conventional reference system (A.) and the proposed solar exoskeleton construction system in steel (B.) and timber (C.).*

For the design and evaluation of the solar exoskeleton systems, we propose an integrative design workflow that includes metrics for embodied and operational carbon in the early stages of design. We present an automated protocol for linking structural simulation and sizing algorithms with solar gain control evaluation and energy simulation.

# 3. Background

## 3.1. Architectural exoskeletons

Architectural exoskeletons have been used in large-scale buildings to create both expressive building geometries and column-free interiors that enable flexible space layouts. They are often designed to use innovative construction methods that go beyond standardized concrete and steel framing constructions. The Centre

Pompidou in Paris, designed by Renzo Piano and Richard Rogers and engineered by Peter Rice in 1971, achieves column-free interiors through a custom cast and prefabricated steel superstructure (Baudrillard 1982). The 1986 Hong Kong and Shanghai Bank (HSBC) Headquarters, designed by architect Foster and Partners and engineered by Arup, consists of an open floor plan office high-rise with a 200m steel framed exoskeleton, without a concrete core (Foster + Partners 1986). The Morpheus Hotel, the first free-form high-rise exoskeleton, was completed in 2018 by Zaha Hadid Architects. Its aluminum-clad exoskeleton façade served as the building's structure and provided additional shading effects to the fully glazed façade (Zaha Hadid Architects 2018). In the 62-story residential tower "One Thousand Museum" by Zaha Hadid Architects, finished in 2020, glass-fiber reinforced concrete panels were used as lost formwork system to cast-in-situ a concrete exoskeleton for hurricane resistant lateral bracing and structural loads (Zaha Hadid Architects 2020).

Exoskeleton structures create a thermal bridge in a building envelope, allowing heat to flow through conductive materials between the external structure and internal structure of the building. This requires careful consideration and detailing of the connections to avoid thermal issues. A number of engineering solutions have been developed and applied successfully to create a thermal break in continuous structural members, such as fiber reinforced polymer and neoprene pads (Hamel and Peterman 2019). In addition, high-strength non-metallic carbon fiber thermal break shims have been used to connect the steel exoskeleton of a six-story commercial development in New York City (with a LEED Gold certification) to its floor plates (Vancura 2014). This paper assumes the deployment of such technologies in its results.

## 3.2. Design optimization for building systems

Computational optimization techniques have been widely applied to building envelopes and environmental design problems (Evins 2013). However, design decisions and performance in the built environment are often difficult to formulate mathematically. New computational workflows are needed to allow goals such as structural efficiency, embodied energy, or cost to be paired with qualitative architectural constraints (Mueller and Ochsendorf 2015). Occupant comfort and energy usage can be taken into account directly when analyzing different building systems, such as facades, based on performance in an optimization process (Minaei and Aksamija 2020). Navigating multi-variable design spaces of buildings can include negotiating between different directly conflicting design variables (Wortmann and Fischer 2020), which requires in-depth study and comparison of the Pareto fronts (Brown, Tseranidis, and Mueller 2015). To negotiate between competing metrics in whole building optimization, compound performance scores can be obtained as a combination of structural and environmental concerns (Turrin et al. 2012; Buelow 2014; Bernett, Kral, and Dogan 2021) daylighting and energy (Mcglashan et al. 2021), solar gains and view (Oswald 2021) or daylighting and building shape (Peters et al. 2019; Jayaweera, Rajapaksha, and Manthilake 2021; Shi, Fonseca, and Schlueter 2021; Konis, Gamas, and Kensek 2016). Furthermore, surrogate modeling techniques can be used for environmental building analysis, increasing parameter spaces while lowering computational costs (Westermann and Evins 2019). These have been applied to investigate embodied carbon based on building shapes (Zargar and Brown 2021). These techniques have been proven functional in a variety of building systems, but have not yet been used for solar exoskeletons.

External shading systems and louvers can have a large impact on the thermal performance of a building, especially in hot climates with high solar radiation. Optimal dimensioning allows for shading during warm periods to prevent overheating, while admitting beneficial solar gains during colder seasons, as well as glare reduction (Fan, Liu, and Tang 2022). Multiple generative systems to aid in the design of shading devices to improve thermal performance in any location have been proposed(Sargent, Niemasz, and Reinhart 2011; Manzan 2014; Marsh 2003; Tang and Landis 2021; Oswald 2021). Furthermore, machine learning algorithms have been utilized to compute optimal orientation of high resolution shading fins across a skyscraper façade (Ekici et al. 2021). The outputs resulted in both optimal shading geometries for louver systems and validated energy models, highlighting the building performance benefits. However, the shading geometries were only materialized without loadbearing function (Bechthold et al. 2011). On a building scale, representation such as Building Information Modeling (BIM) allows for limited parametric adjustments of window size and global

geometry to be considered in multi-objective optimization workflows (Asl et al. 2014). Using variation in building geometries and construction buildup, multi-objective approaches can further be used to minimize the total building energy for a specific climate and urban context (Méndez et al. 2015; Zhao and Du 2020).

Freeform shading systems have been studied geometrically and for their solar gain control performance (Tang and Landis 2021). Jiang and Wang investigated the geometric optimization of planar quads surfaces to block light from given sun angles while maintaining certain constraints (Jiang et al. 2013; Wang et al. 2013). Geometric flexibility and stability are considered in the creation of torsion-free structures from planar strips, but they remain constrained to the model-making scale. Based on the sculptor Erwin Hauer's screen designs, Omidfar analyzed how parametrized and geometrically complex shapes could be used as performative shading devices (Omidfar 2011). Variability of form was coupled with solar radiation performance simulations and compared to traditional, fully glazed façades without a secondary screen. To compare different complex shading screens, a spatio-temporal map was proposed to quantify total annual irradiation (Mardaljevic 2003). Although used as façade or ceiling elements, the structural and material properties of the screens were not considered.

### 3.3. Research Scope

This paper's research expands on the combination of parametric geometry with structural optimization and solar simulation techniques. Going beyond abstract geometric representations for structural and solar simulations, we work on a detailed architectural scale. Even though optimal shading geometries have been the subject of extensive research, their usage as structural systems has not been studied. Furthermore, in contrast to existing research, we are integrating materiality and element sizing as a key factor in the digital design and structural optimization processes.

## 4. Methods

We combine tools from the environmental simulation domain with structural analysis methods and parametric modeling techniques. We test our simulation and analysis methods on two case study office buildings: a prototypical 10-story midrise building and a 25-story tower. The automated workflow was implemented in the architectural CAD software Rhino and its integrated scripting platform Grasshopper utilizing custom Python components, the structural analysis package Karamba3D (Preisinger and Heimrath 2014) and EnergyPlus (Crawley et al. 2000) through the Climate Studio package (Solemma 2021). While applied to quantify the solar exoskeleton system, our workflow could also be used to quantify the effects of regular building scale shading systems.

The automated workflow, as described in Figure 2, starts with a parametric façade model. In the definition of the exoskeleton geometry, the density and connectivity between the beam members can be adjusted and their materiality defined. The line model is transferred to Karamba3D where members are analyzed and dimensioned according to building code-prescribed structural calculations, and a structural mesh is produced that represents the volumetric geometry the structure.

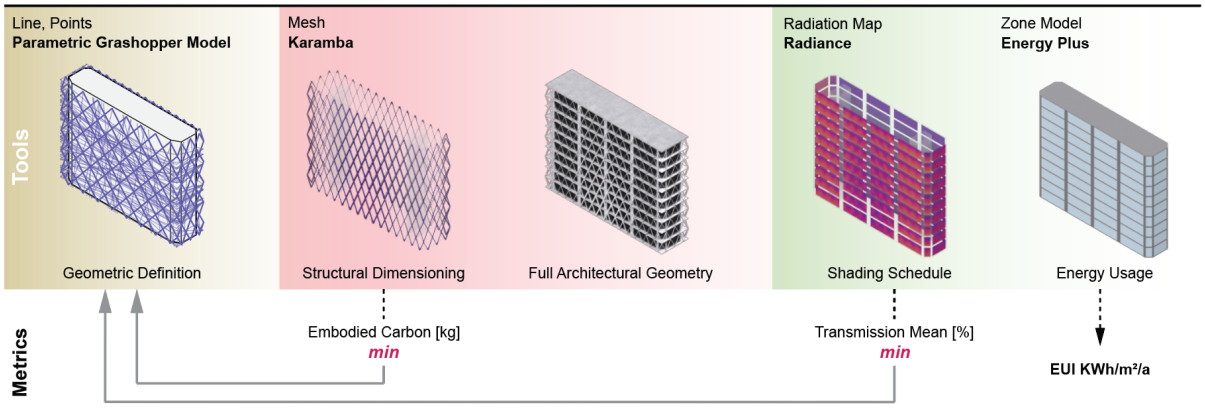


*Figure 2: Overview of the automated workflow including the software tools and evaluated metrics.*

This serves as the basis for the full architectural geometry that includes optional shading fins and floors connected to the loadbearing exoskeleton layer on the outside of the building. The full architectural geometry is then used to calculate precise hourly solar gains onto all window surfaces throughout the year. This information is used by an EnergyPlus simulation of the Energy Use Intensity (EUI) of the building. All simulations were conducted on a Windows computer with the following specifications: 64 GB Ram, Nvidia GeForce GTX 1080 Graphics card, Intel(R) Core(TM) i7-6700K @ 4.0 GHz Processor. The structural sizing optimization of a single full-scale building variant took 1-5min, while the full radiation and energy simulation required 3-14min of calculation time, depending on the complexity of the structure. The details of this overall approach for solar exoskeleton design and simulation are provided in the following sections.

## 4.1. Design and parametric geometry generation

The 10-story midrise building and the 25-story tower, described in Figure 3, serve as the basis for the parametric façade and structure creation. The buildings represent two prototypical office developments in an environment without any shading from other buildings. It should be noted that neighboring context with arbitrary geometric detail could be added to the solar radiation simulation step with limited impact on model setup and simulation time. In the midrise building, two structural concrete cores of 6.5m x3.5m serve as a vertical circulation area (stairs and elevators) between floors while the tower design features a single core of 12.5m x 11m. A fully glazed façade with a window-to-wall ratio (WWR) of 80% represents the reference façade system for both designs.

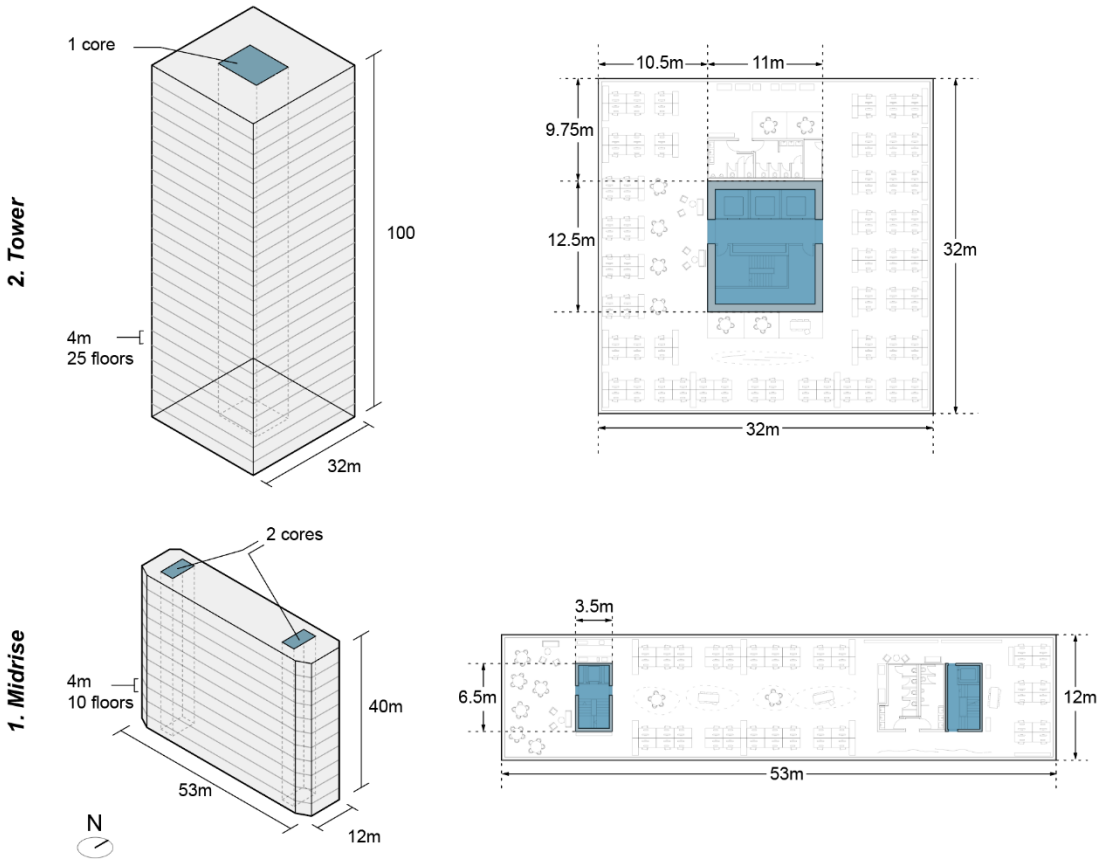


*Figure 3: Overview of building dimensions, and orientation to North (N) of midrise (1.) and tower (2.) structure*

Several exoskeleton typologies were considered in this work, ranging from more typical to more irregular. Each exoskeleton is composed of a system of connected structural elements with specific geometries generated through defined parameters that control the density, direction, and connectivity between elements. Variable seed ratios for random beam distribution were used to generate different versions of the same element distribution. The resulting element layouts are initially material-agnostic and purely geometric, serving as an input to be dimensioned and processed for two separate construction material solutions, timber, and steel. In addition to the loadbearing element geometry, additional shading fins for the south, east and west façades were added. As described in Figure 4, a regular diagrid with variable element spacing as well as a series of scattered angled grids with varying densities were evaluated. Both horizontal and vertical subdivisions, as well as coarse and sparse element layouts, resulted in a diverse dataset in terms of shading properties and structural efficiency. Diagrids and element scattering could be controlled in high detail in terms of beam angles and distribution ratio.

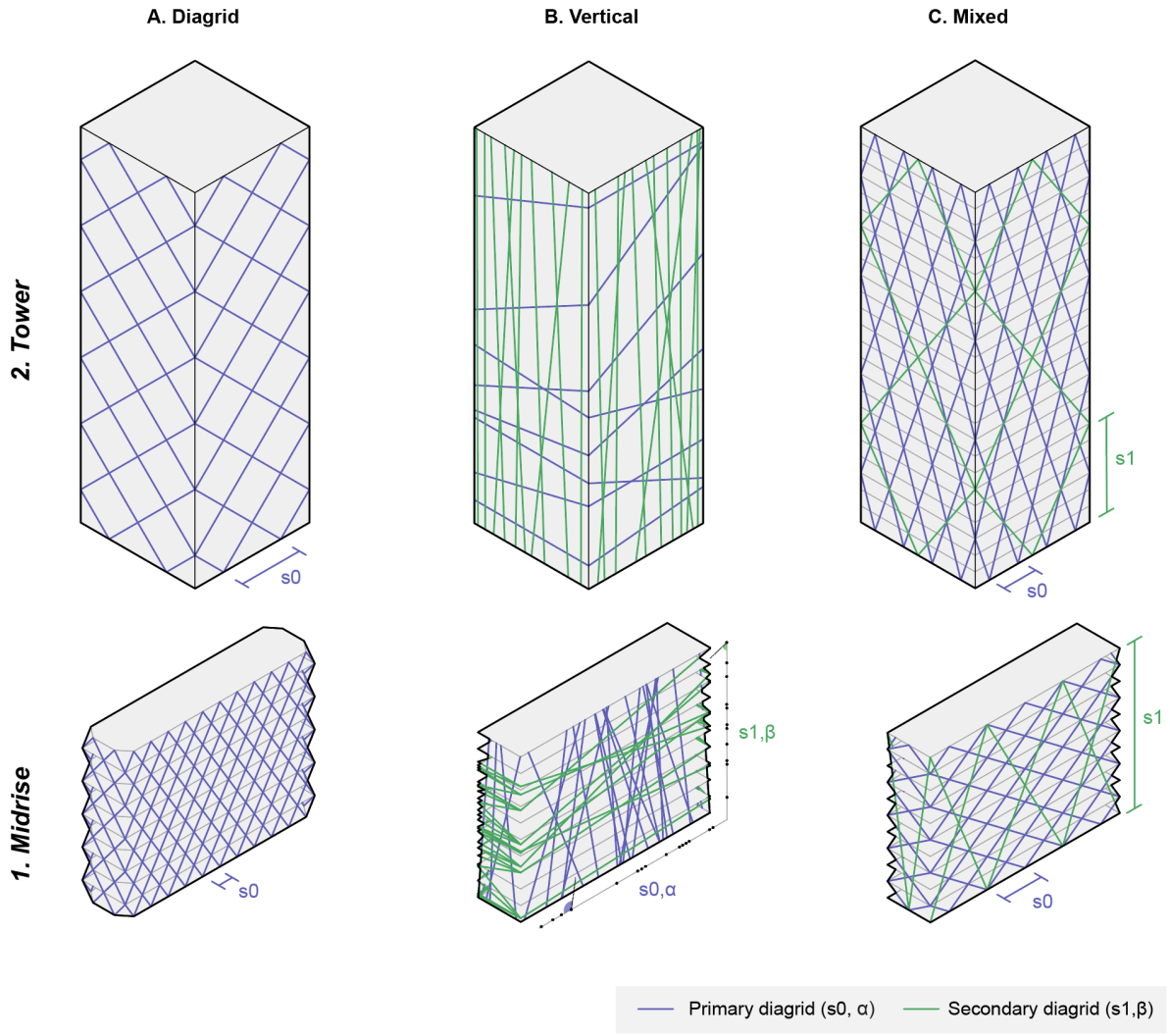


*Figure 4: Geometric definition with floors and beams of a single diagrid (A.) with variable spacing (s0). Vertical scattering (B.) with two overlaid diagrids with variable beam angle (a, β) and variable spacing (s0, s1) and mixed scattering (C.) with two overlaid diagrids with variable spacing (s0, s1).*

## 4.2. Dimensioning of building components and structural simulation

The finite element analysis tool Karamba3D (Preisinger and Heimrath 2014) was used as the structural analysis and sizing component in the parametric feedback loop. Its implementation in the software Rhino allows for an interface with environmental and geometric constraints. The parts of the prototypical building were defined as outlined in Table 1. Floors and shafts of the cores are materialized in reinforced concrete while the exoskeleton's columns feature variable hollow rectangular tube steel and solid rectangular timber cross sections. The automated dimensioning process described above is used to calculate material quantities for embodied carbon estimation, as discussed in Section 4.5.

The structural system was modeled with mesh elements for floor slabs and core walls and linear elements for exoskeleton members. Structural simulation and loading parameters are described in detail in Table 3. The wind load was applied to a bounding box mesh of the building geometry, in addition to a reasonable estimate of dead and live loads due to gravity. The Karamba3D internal function of cross-section optimization was used to choose between a select range of possible dimensions for the structural elements

*Table 1: Overview of building components*

| **Building Components** | **Material** | **Dimensions [cm]** |
|---|---|---|
| *Floors* | Concrete | 30 cm deep (fixed) |
| *Shaft* | Concrete | 30 cm thick (fixed) |
| *Columns (Exoskeleton & Reference Case)* | Steel | Rectangular Hollow: Height 2.5-300 / Width 2.5-30 / Thickness 1 cm |
| | Timber | Rectangular Solid: Height / Width 10-300 cm |
| *Shading fins* | Aluminum | 0.25 |

*Table 2: Material specifications for the structural simulation and embodied carbon estimation from the ICE database (Jones and Hammond 2019). Coefficients from worldwide averages (*) and USA specific EPD averages.*

| **Material Specifications** | **Steel** | **Concrete (with steel rebar)** | **Timber** | **Aluminum** |
|---|---|---|---|---|
| *Elastic Modulus [kN/cm$^2$]* | 21000 | 3100 | 1050 | (not included in structural |
| *Shear Modulus [kN/cm$^2$]* | 8076 | 1291.67 | 360 | simulation) |
| *Density [kg/m$^3$]* | 7850 | 2400 | 530 | 2750 |
| *Embodied Carbon Coefficient (ECC) [kgCO2e/kg]* | 1.55 * | not used | 0.493 * | 5.65 (USA) |

*Table 3: Structural simulation inputs (Karamba)*

| | | |
|---|---|---|
| **Wind Pressure (Load Case 0,1,2,3 four different sides)** | 2.5 kN/m2 | |
| **Live and Dead Loads** | 2g (amplification of self-weight by a factor of 2 to account for additional un-modeled live and dead loads) | |
| **OptiCroSec (Karamba3D sizing function)** | Ultimate Limit State Iterations ULSIter | 10 |
| | Displacement Iterations | 10 |
| | Max Displacement | Building height/400 |
| | nSamples | 3 |

A reference structure shown in Figure 5 was also modeled for comparative purposes; this structure uses a traditional beam-column gravity frame with a braced frame lateral system; this is the conventional building typology represented in Figure 1a. The workflow from structural model to beam dimensioning and the final architectural geometry is visualized in Figure 6. A sample of the direct comparison of member sizing between different steel diagrid iterations is shown in Figure 7, where the spacing of the diagrid members was adjusted iteratively from 1-10m.

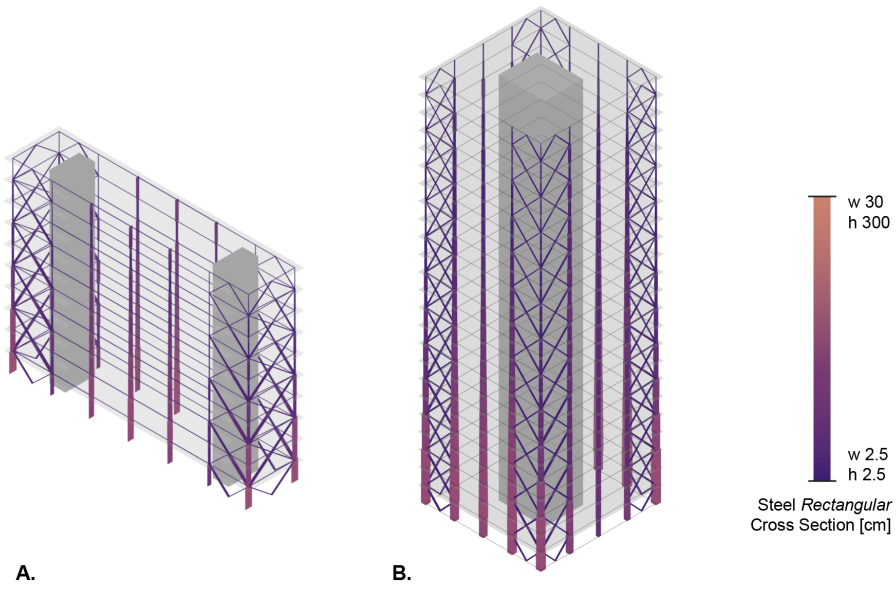


*Figure 5: Reference structure of midrise (A.) and tower (B.) with internal column grid, core, and cross-bracing.*

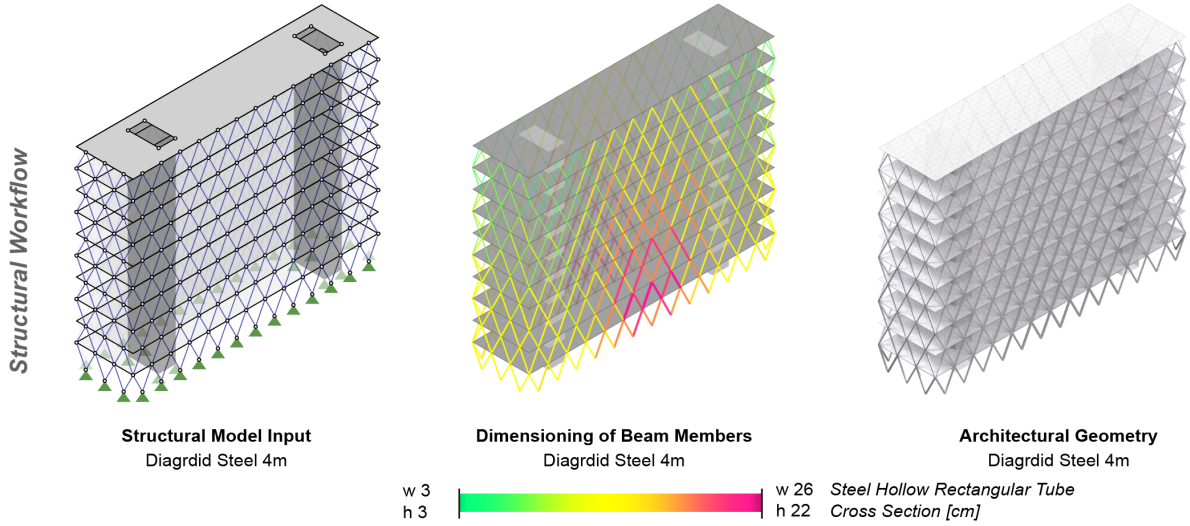


*Figure 6: Structural workflow outlined with the inputs for the structural model (top). A representation of the structure with points, lines, and supports that is dimensioned and results in the final architectural geometry.*

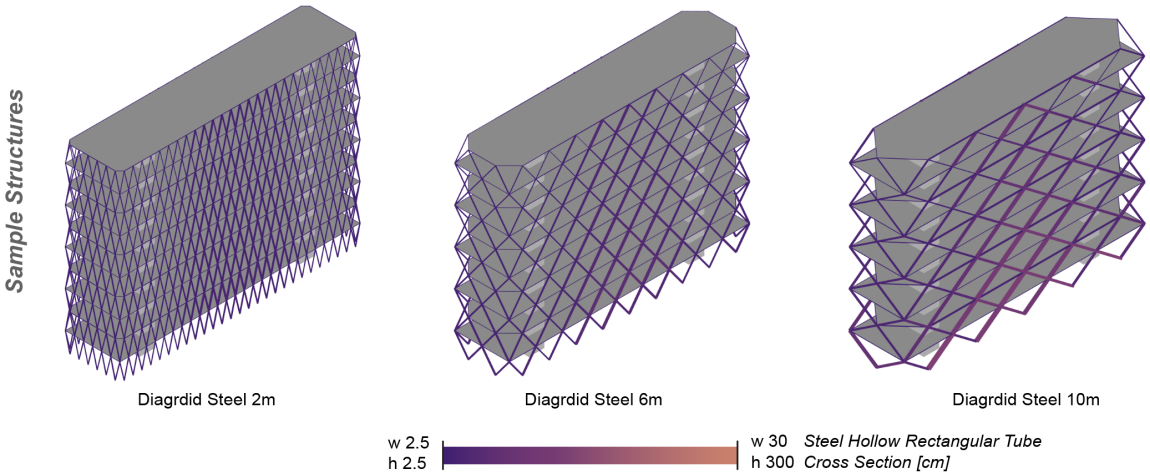


*Figure 7: Three sample structures in steel with node spacing (s) of 2m, 6m and 10m. Element members are colored according to the largest and smallest member to display the mass distribution.*

## 4.3. Architectural geometry

We construct the final architectural geometry to be used for the shading calculation based on the structurally dimensioned exoskeleton. As the structural elements would have to be fire clad and weatherproofed (in the case of steel), we add an additional 3cm offset to the beam members. In optimal structural form, the members of the exoskeleton are as slender as possible, which is in turn suboptimal for shading purposes. To mitigate this, we extend the beam cladding on the south, west and east façades, offset to the normal direction of the underlying façade surface. Unlike more conventional architectural solutions, a secondary supporting structure for the shading fins is not necessary. The geometric details of the post-processing methods are described in Figure 8.

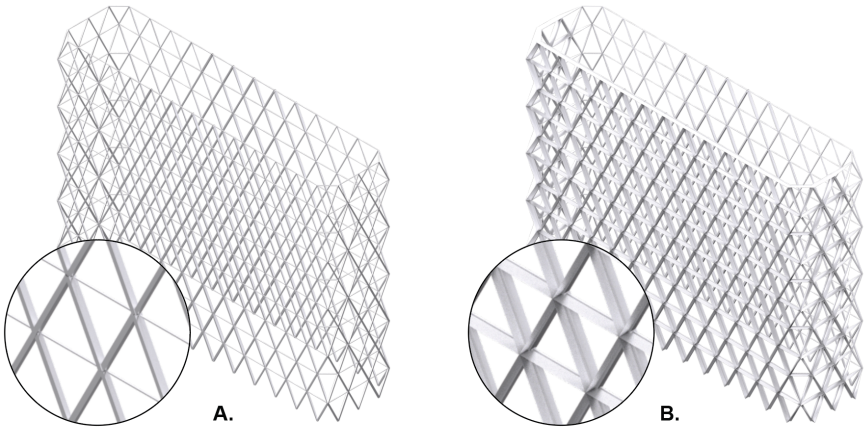


*Figure 8: Exoskeleton geometry as only the structure (A) and with extended fins (0.8m).*

## 4.4. Shading and energy simulation

The dimensioned beams output by the structural simulation were further used as input for custom shading coefficients in EnergyPlus. To process the complex shading geometry in EnergyPlus, we calculated the hourly shading coefficient caused by the exoskeleton as the ratio of the solar radiation onto the façade with the exoskeleton geometry to the radiation onto the unshaded façade. Inspired by existing workflows (Omidfar 2011) and the Spatio-Temporal Irradiation Mapping workflow (Mardaljevic 2003), we created an automated procedure

to calculate mean shading transmission coefficients for each window of the building. The irradiation map calculations are based on annual Radiance simulations using ClimateStudio (Ward, G. and Shakespeare 1998). The detailed radiation map underlying the calculation ensures that our geometrically differentiated shading devices are reflected correctly in the radiation map, as they vary from side to side and throughout a single façade plane. Radiation maps for a shaded and unshaded façade were calculated on each façade face on a single floor (fifth floor in the midrise and tenth floor in the tower) resulting in a detailed yearly radiation map with a sensor grid with 10cm spacing. The ratio of shaded and unshaded radiation map was used to construct a yearly shading coefficient schedule for each façade side (north, south, east, west) for every hour of the year. This schedule was used for each corresponding façade orientation assuming an exterior shading device in front of each window in the EnergyPlus simulation. Figure 9 gives an overview of the energy simulation. As described in Table 4, we assume that the thermal performance of the building is exemplary with optimized internal loads, located in Phoenix, AZ, USA, and supplied by an all-electric heat pump heating and cooling system with COP 4.6.

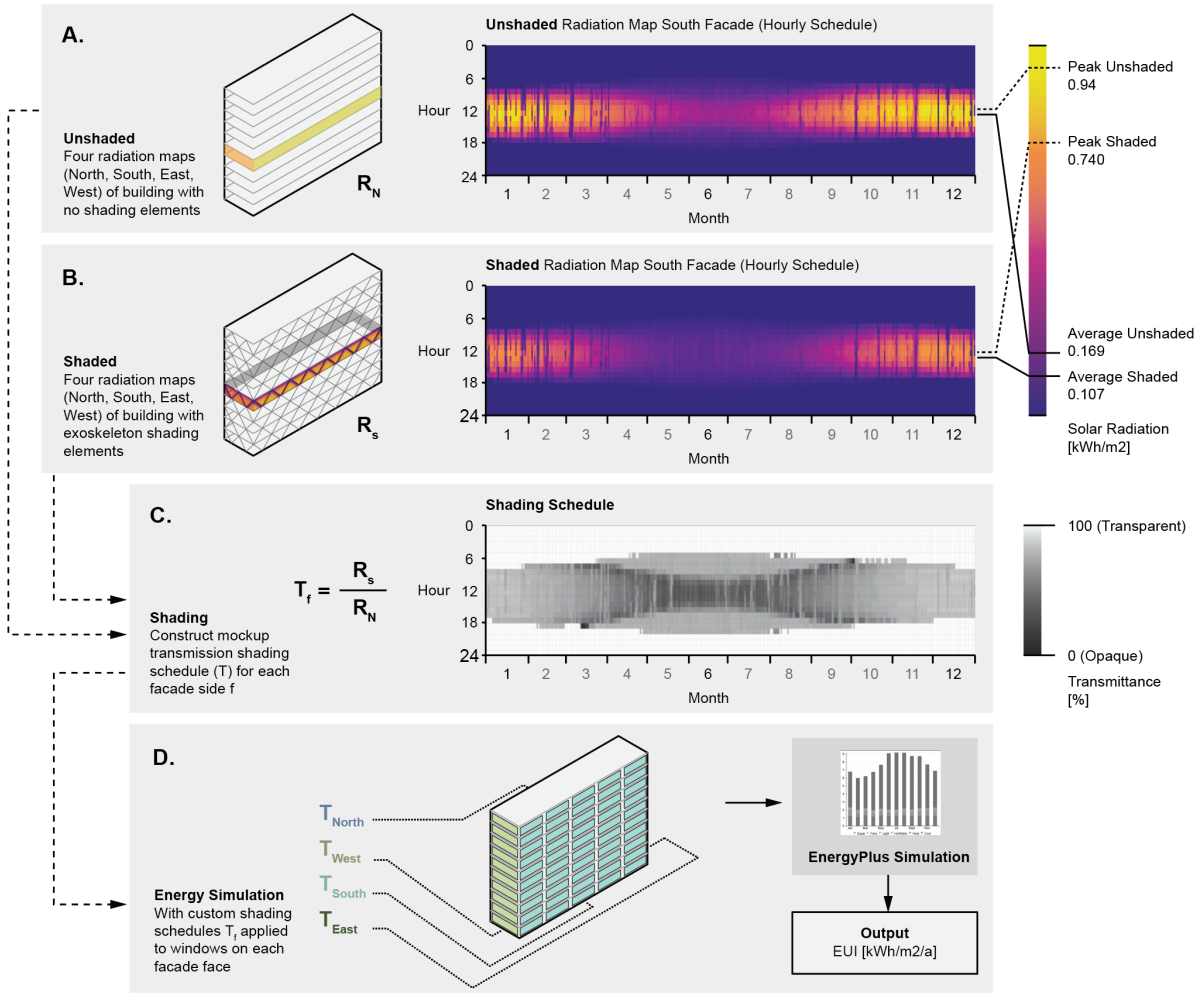


*Figure 9: Overview of energy simulation that is able to capture the effects of complex exterior shading systems. A radiation map for a typical floor on each façade is calculated with Radiance (A.) using no shading obstructions. The shading elements are included in the geometry to create a radiation map with shading (B.). From the two radiation maps a shading schedule is produced (C.). The schedule is used as custom shading coefficient schedule on all windows of each side of the building (D.) and input into EnergyPlus for the final EUI generation.*

*Table 4: Energy simulation inputs (EnergyPlus/Climate Studio). Location and emission factors variable as stated.*

| | |
|---|---|
| *Location* | Phoenix, AZ, USA |
| *Zone Settings* | Office |
| *Lighting* | Dimming/LED |
| *HVAC* | Electric HP COP4,6 including Heat Recovery |
| *Electricity Emission Factor CO2[kg/kWh]* | 0.685 |
| *Simulation Mode* | Simple Zone Airflow |
| *Solar Distribution calculation* | FullInteriorAndExteriorWithReflections |
| *Glazing* | TriplePaneLoE (U-value 0.785 W/($m^2$K)*)* |
| *Shading* | (No Shading by Default) |
| *Wall U-Value [*W/($m^2$K)*]* | 0.1 |
| *Window To Wall Ratio (WWR)* | 0.8 |
| *Thermal Mass* | _Mass |
| *Radiance settings for radiation map* | -ab 6 -lw 0.01 |

## 4.5. Embodied carbon estimation

In this paper's embodied carbon estimation, we restrict ourselves to the materials of the dimensioned building's lateral load-resisting structural system, often just referred to as the lateral system: the solar diagrid exoskeleton, or in the case of the reference building, the columns and bracing structure. The central structural core and the structural floor system were not incorporated in the embodied carbon comparison, as they are the same in all designs, although their mechanical contributions to the building's structural behavior were accounted for. It is also important to note that the design of the solar exoskeleton is independent of the choice of structural floor system, which can vary significantly in mass and carbon content. It is therefore both simpler and more accurate to exclude these other systems from our comparative carbon emission analysis. A tall building's lateral system has been found to contribute substantially to the total embodied carbon of a structure (although its precise percentage depends on choices made beyond the scope of this paper): Foraboschi highlights the significant contributions of lateral and wind load systems to the embodied carbon content of tall buildings with the latter exponentially growing with building height (Foraboschi, Mercanzin, and Trabucco 2014).

This paper uses a process-based Life Cycle Assessment (LCA) analysis, a common method with reliable databases (Moncaster and Song 2012), that uses material-quantities for embodied carbon estimation. As shown in Section 4.6, material quantities resulting from automated structural calculations are multiplied by embodied carbon coefficients for each material, and summed over the full building system. Also referred to as cradle-to-gate material coefficients (comparable to the LCA Stages A1-A3, according to EN 15978:2011), this approach encompasses the production and manufacturing of the building materials. We exclude the transport and construction (LCA stage A4-5) and use stage (LCA stage B) as they are hard to predict and do not impact the embodied carbon of the structural frame significantly (Hart, D'Amico, and Pomponi 2021). Compared to low-rise buildings, end of life (LCA stage C) and reuse (LCA stage D) in tall buildings include very high uncertainty as economic pressure and uncertain real-estate markets can shorten the service life of a building significantly (Gan et al. 2017; Trabucco and Belmonte 2021). Furthermore, there is very limited data on intentional demolition of very tall buildings (Trabucco 2016). We exclude the envelope, floors, central core, foundation, and fit outs to allow for comparative analysis between only the building's vertical structure, allowing for early-stage ideation and a generalized understanding of the solar exoskeleton carbon intensity independent of other building systems.

As environmental product declarations (EPD) published by industry can vary greatly with severe inconsistencies (Anderson and Moncaster 2020) we use worldwide averages (for steel, concrete and timber) and US specific averages (aluminum) from the ICE database (Jones and Hammond 2019). Even though our case study simulates a building in the U.S., the worldwide averages are within the uncertainty thresholds of aggregated U.S. EPD's (Building Transparency 2021; American Institute of Steel Construction 2021). The material coefficients used in our simulations are described in detail in Table 2.

## 4.6. Performance metrics

Based on these simulation methods, two key performance metrics are recorded for a range of parametrically generated exoskeleton designs:

1. *Embodied carbon of exoskeleton structure*: This metric, normalized by the total floor area *A* of the building, is calculated as follows:

$$\text{Embodied carbon} = \frac{\sum_{i=0}^{n} V_i \rho_i \, ECC_i}{A}$$

Where V is the total material volume of the sized structure, $\rho$ is the material density, and ECC is the embodied carbon coefficient (from Table 2) for each of the *n* materials used in the structure. This metric, measured in kg-$CO_2e/m^2$, is a key measure of the carbon impact of the building's materials, and is often referred to as the global warming potential (GWP) of a design

2. *Energy use intensity (EUI) of the whole building*: This metric measures the electricity use in kWh of a building per year normalized by the floor area. It is calculated via a full energy simulation (section 3.4) and output in units of $kWh/m^2$

# 5. Results

The following sections describe the results of the structural simulations, comparing the embodied energy of different material solutions. We further study the impact on the operational energy of the different shading systems and compare them with a reference structure in terms of weight of loadbearing structure and EUI. The parametric architectural geometries also produced structures that were not structurally valid, with components exceeding the maximum member sizes. These were excluded from both embodied carbon and EUI calculations.

## 5.1. Embodied carbon results of materialization and structural simulation

The three geometric exoskeleton typologies – the diagrid, vertical scattering, and mixed diagrids – were assessed in both steel and timber as the loadbearing material are outlined in Figure 10 and in Figure 11 for the midrise typology and for the tower typology, respectively. Due to better distribution of lateral loads, both exoskeleton solutions save a substantial amount of material and carbon when compared to the reference case. In a best-case scenario, the generated structural exoskeletons use 64% of the embodied carbon compared to the reference in the steel case, and 20% of the embodied carbon in the timber version. The most efficient steel element layout performed comparably to the lower performing timber iterations with large spans. The solid timber cross sections in comparison to the hollow rectangular steel tubes are significantly larger; however, due to the much lower embodied carbon of timber, they perform better in the comparative analysis. Detailed results of the embodied carbon savings of the exoskeleton systems when compared to the reference building are outlined in Table 5.

*Table 5: Best case scenario embodied carbon savings compared to the reference structure. In percentage of the embodied carbon of the midrise (27.6 kgCO2e/m2) and the tower structure (35.5 kgCO2e/m2) in steel and timber*

| **Minimum EC in % of reference structure** | **Midrise** | | | **Tower** | | |
|---|---|---|---|---|---|---|
| | Diagrid | Vertical | Mixed | Diagrid | Vertical | Mixed |
| *Steel* | 68.5% | 84.8% | 39.5% | 63.6% | 133.2% | 69.8% |
| *Timber* | 24.9% | 23.9% | 20.4% | 31.9% | 59.5% | 32.2% |

## 5.2. Energy Use Intensity and tradeoff with embodied carbon

As a final step in the workflow, a radiation analysis of the solar gains from the glazed façade is conducted to generate shading transmission coefficients. The coefficient is further used in the energy simulation to estimate

the building's EUI. We compare the results with our reference building without shading and an internal structure that resulted in an EUI of 88.5 kWh/$m^2$ in the midrise tower and an EUI of 68.1 kWh/$m^2$ in the tower structure. In the best-case scenarios of shaded structures with a solar exoskeleton, the tower structure achieves an EUI of 45.3 kWh/$m^2$, 66.5% of the reference structure. In the midrise structure the lowest EUI was computed at 46.4 kWh/$m^2$, 52.5% of the reference. The EUI simulations of the steel structure were conducted with aluminum fins and cladding around the steel members. This additional embodied carbon from the aluminum is substantial and increases the total embodied carbon significantly. EUI results are compared to their corresponding embodied carbon emissions in Figure 12 in a bi-objective plotting style commonly used in multi-objective optimization. The results reveal the opportunity for high-performance designs in which minimal EUIs can be achieved without large penalties in embodied carbon. In other words, a traditional Pareto frontier with tradeoffs between objectives is not especially pronounced, and both operational and embodied carbon priorities can be addressed simultaneously with a well-designed solar exoskeleton. Designs that perform especially well in both objectives tend to have mixed or diagrid topologies and more frequently spaced elements, although the advantage of density diminishes after threshold values as shown in Figure 10. This is likely because design instances with more structural exoskeleton elements not only offer more shading, but also can lead to overall reduction of mass as they perform more efficiently as a structural system and the smaller individual member sizing offsets the structural mass gain by an increase in the overall number of elements.

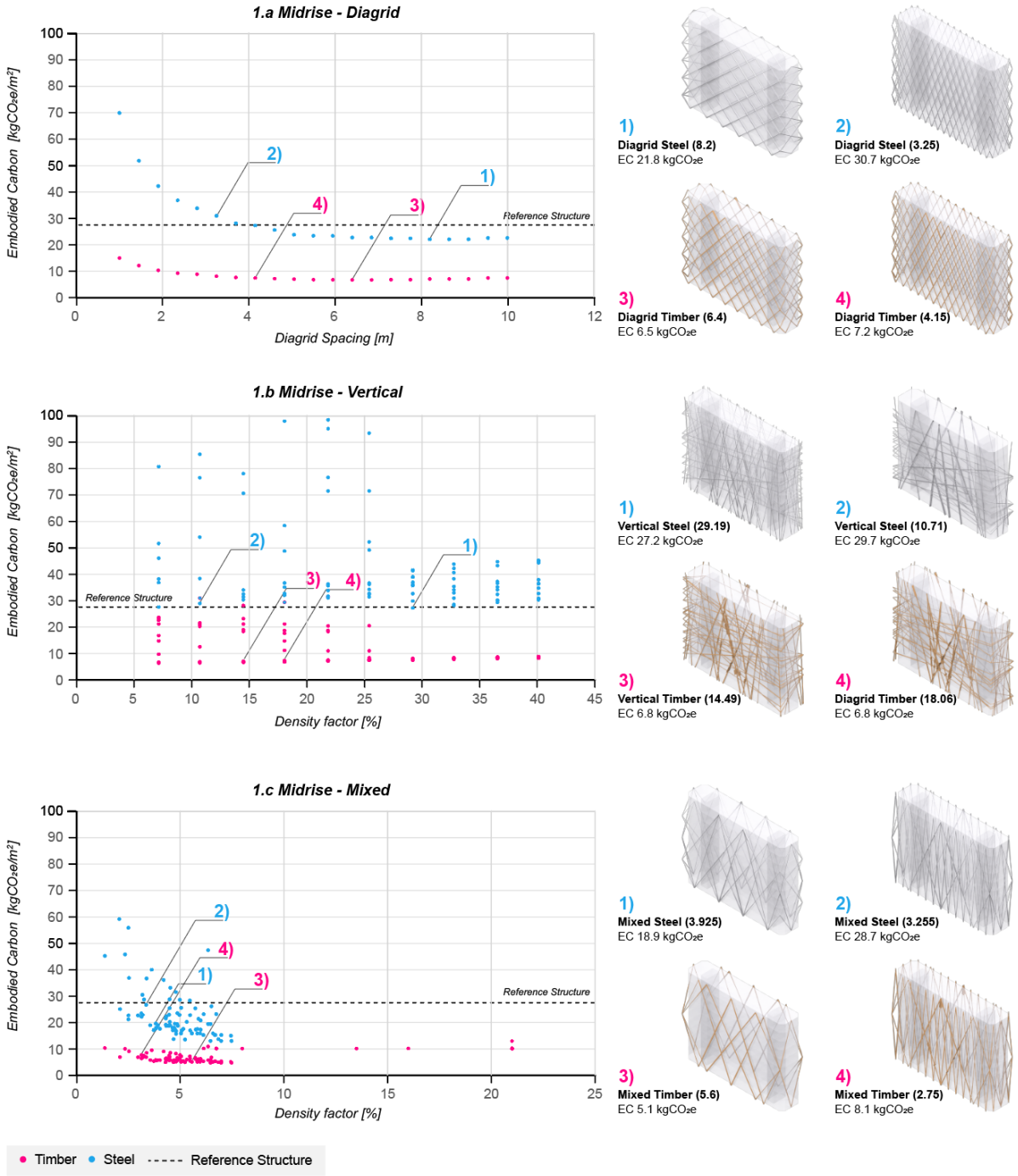


*Figure 10: Embodied carbon, normalized per floor area, of the three geometric exoskeleton geometry types in steel and timber of the midrise typology. Diagrid with 37 samples (1.a), Vertical with 182 samples (1.b) and Mixed with 35 samples (1.c).*

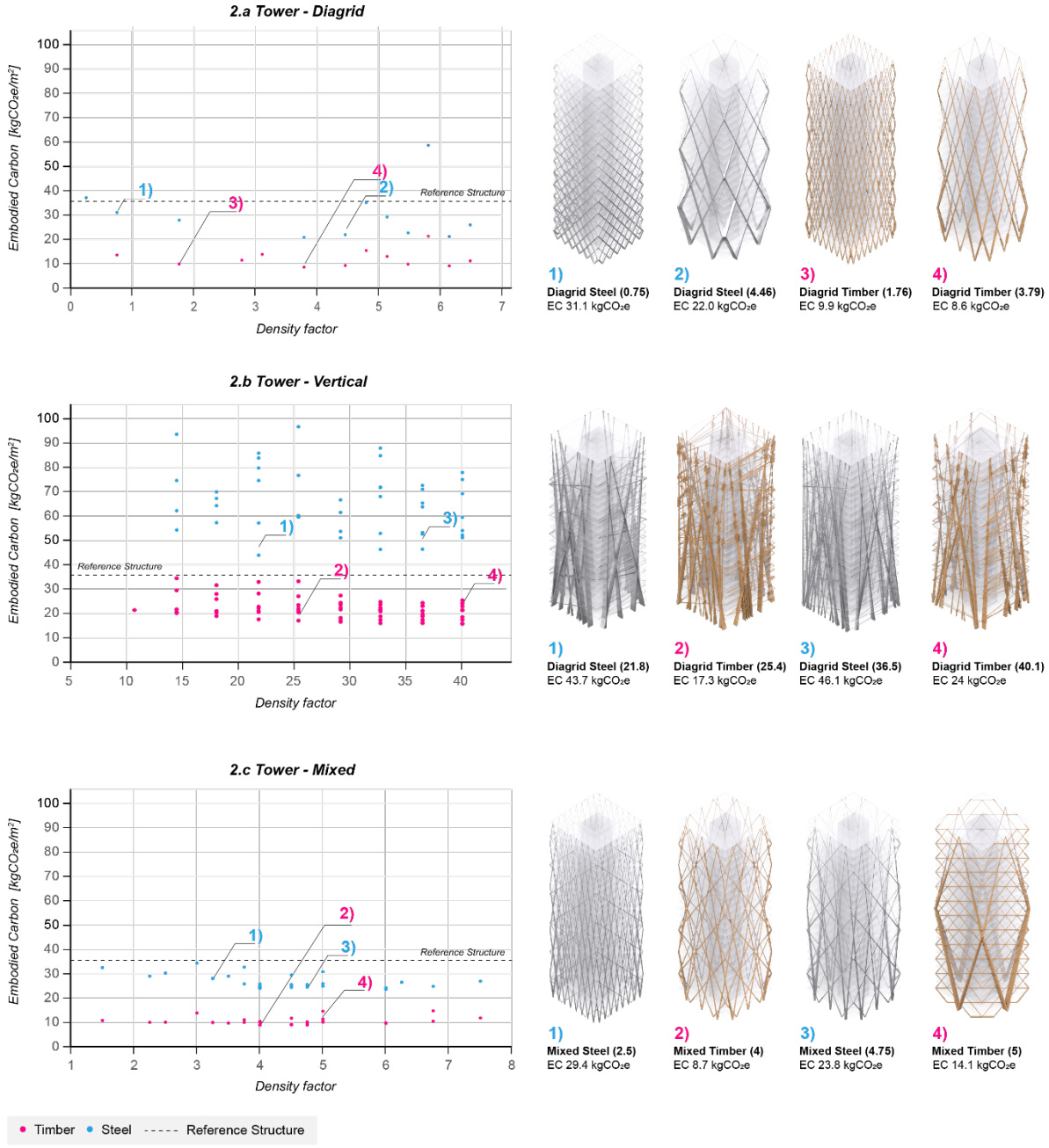


*Figure 11: Embodied carbon, normalized per floor area, of the three geometric exoskeleton geometry types in steel and timber of the tower typology. Diagrid with 21 samples (1.a), Vertical with 65 samples (1.b) and Mixed with 60 samples (1.c).*

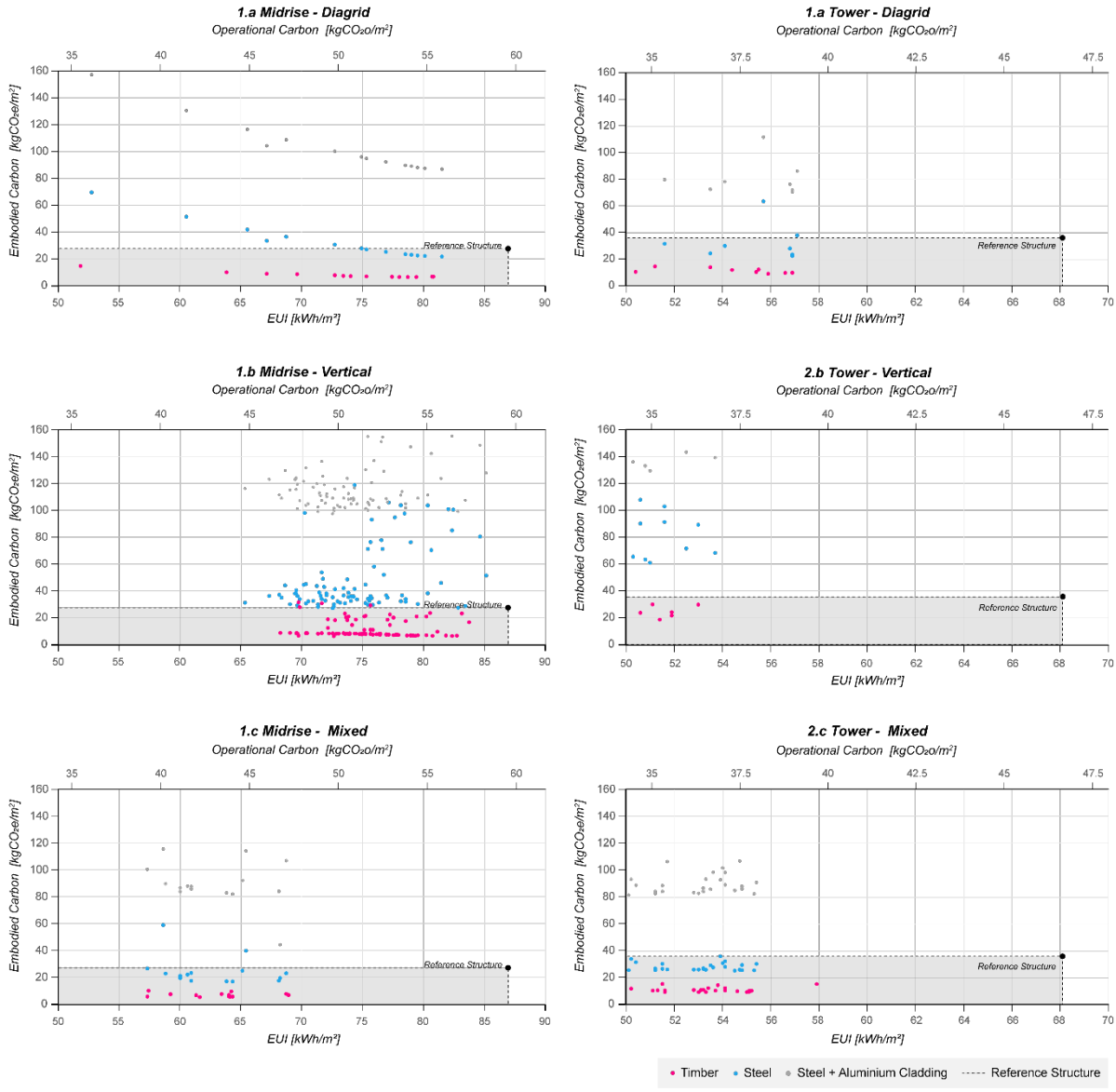


*Figure 12: Embodied carbon normalized per floor area with corresponding EUI and operational carbon resulting from the energy simulation. The results of timber, steel, and steel structure with aluminum cladding for the fins.*

## 5.3. Impact of grid decarbonization on carbon emissions

To visualize the impact of the EUI reduction on lifecycle emissions, we evaluate the building's operational carbon emissions with multiple grid scenarios. We compare cumulative carbon emissions of three scenarios: the status quo, a linear decarbonization of the grid from 2030 to 2050 and a rapid decarbonization of the grid from 2025-2035. As shown in Figure 13, savings of the shading amount to 2.3 to 8 years of operational energy of a structure, and the carbon gains are 3.6 to 12 times higher than the embodied carbon of the building's vertical structure.

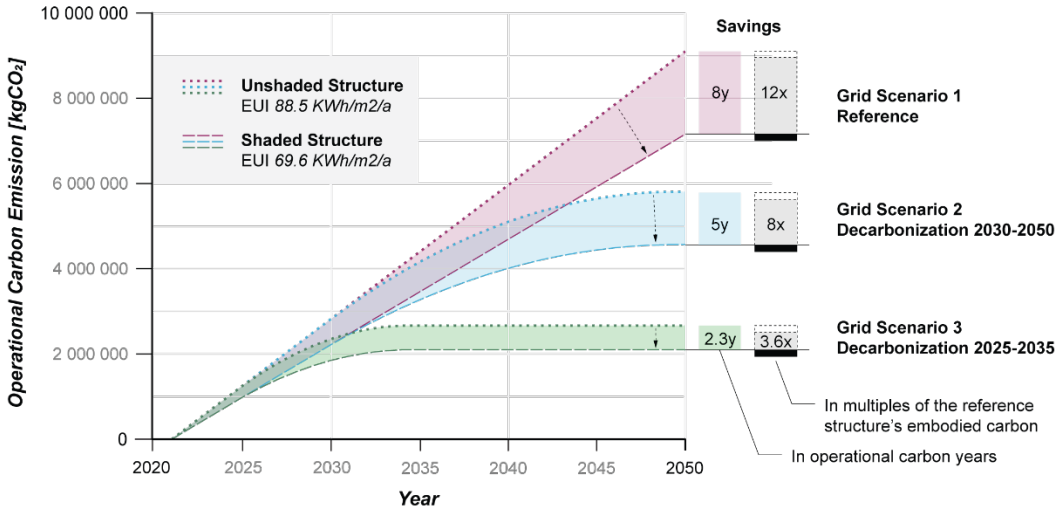


Figure 13: Operational carbon emission of an exoskeleton structure with average EUI in multiple grid scenarios. Carbon savings due to the solar exoskeleton are shown as multiples of the reference structure and operational carbon years.

## 5.4. Achieving net zero with onsite photovoltaics (PV)

To assess the impact of the reduction of EUI on the potential for building a net zero structure, we computed samples for both midrise and tower buildings and explored their electricity production potential. As revealed in Table 5, rooftop PVs were able to cover 52.6% of the electricity required in the case of the midrise building and 34.8% in case of the tower building. Considering minimum and maximum EUI, 44.8% - 82.2% of electricity use could be generated by rooftop PVs. In a second step, we considered the shading fins as mounts for solar panels, as shown in Figure 1. For both building typologies with an average building in terms of EUI, net zero energy use was achieved while generating 134% (midrise) and 127.1% (tower) of the annual electricity onsite.

*Table 5: On site electricity production through rooftop and façade PV-System for sample midrise and tower building with diagrid shading, with Climate Studio PV Simulation Parameters: Efficiency 0.2206, Effective Area 0.8, Sample A. (6000 m2 floor area, Diagrid 3.25 with fin area of 1949 m2) and Sample B. (23600 m2 floor area, Diagrid 5.25m with fin area of 10563 m2)*

| | EUI [kWh/m2/a] | Energy Usage [kWh] | Rooftop PV [kWh/a] | Exoskeleton PV [kWh/a] | Onsite Energy |
|---|---|---|---|---|---|
| *Midrise A.* | **72.6** | **435600** | 228957 (52.6%) | 354686 (81.4%) | 134.0 % |
| *Tower B.* | **51.6** | **1217760** | 424157 (34.8%) | 1123200 (92.2%) | 127.0 % |

With the solar exoskeletons, the structures reduced their cooling loads and through that the overall EUI significantly in the investigated hot climate. A reduction in peak loads is especially important in the larger context of an electric grid where cooling loads are a significant driver for capacity shortages in the summer months. In the optimal scenario of the tower structure (EUI of 43 kWh/m$^2$), the shading reduces the cooling loads in the summer July peak by 20.8% (4.1 to 3.2 kWh/m$^2$) and in the midrise structure (optimal scenario EUI of 46 kWh/m2) by 32.2% (4.6 to 3.1 kWh/m$^2$).

# 6. Discussion

This research proposes an integrated building design strategy linking structural, architectural, and energetic design considerations. On a technical level, we established an automated workflow combining the simulation of a structural exoskeleton and evaluation of its shading impact on energy usage, linking energy, solar and structural simulations with the creation of architectural geometry. Traditionally separate, we propose to conceptually link the design of building envelope with the building structure. The structural exoskeleton not

only creates column-free and flexible interior spaces while also shading the building, in addition to serving as the loadbearing structure.

The results of the research stress the importance of placing sustainability at the core of the design process. We can show how, in the context of building envelopes and structure, optimal solutions that reduce operational and embodied energy can be complementary. Multi-purpose use of building components for both environmental and structural purposes can be enabled by novel computational and generative design workflows. In agreement with previous research, the timber construction systems evaluated in this study exhibit significantly improved embodied energy quantities while performing equally well as their steel counterparts.

Even with significantly higher embodied energy expenses, e.g. in the case of fin systems on steel structures that embody more emissions than our reference structure, our case study buildings make up for higher initial investment in embodied energy through their reduction in operational energy use. In fact, even a doubling of the embodied energy would still result in lower carbon emissions in the most optimistic grid scenario. In the case of optimal timber and steel exoskeletons, the measured embodied carbon was as low as 63.6% (steel) and 20.3% (timber) of the reference structure, while the EUI was as low as 66.5% (tower) and 52.5% (midrise), outperforming the reference case in both embodied and operational carbon emissions.

In the scope of the research, we have only made use of simplified material quantities, compared to a highly detailed life cycle assessment of all building components that would capture the carbon impact of a proposed building in more detail. Furthermore, the carbon impact of more complex non-standard construction has not been included in the comparative analysis. As material quantities for beam members are calculated as non-continuous discrete elements with varying cross sections in continuous beams, issues of joinery have not been addressed. However, state of the art construction in timber and steel suggests that through more digitized planning and fabrication practices, these complexities could be mitigated.

With our simulated building located in ASHRAE Climate Zone 2B (Hot Dry), the studies are foremost applicable to hot climates that are cooling dominated, specifically where heating losses through building envelopes are a lesser concern. The complexity in construction of exoskeletons with minimal thermal bridges in a heating dominated climate would require significant effort in detailing and further study. In the case of timber structures, where thorough fireproofing requires thicker cross sections, claddings or coatings would have to be additionally investigated.

The results show how our workflow can mitigate carbon emissions both short term through lower embodied carbon, as well as long-term through approaching net zero building operation. Achieving net zero not only with the best-case scenario, but through average performing samples, highlights the potential benefits of introducing integrative workflows into architectural design. With electric grids powered by renewables, the reduction of peak loads becomes more important. The shading structures are key in this, delivering low-carbon buildings in cooling dominated areas of the world.

# 7. Outlook

Further research on materialization and constructability could leverage prefabrication and digital manufacturing techniques to enable real-world implementation and built applications of a solar exoskeleton. With its automated nature, the presented workflow can be easily adapted for differentiated design solutions and a plethora of architectural expressions that can take local architectural requirements into account. The creation of material driven workflows can consider local construction methods as well as the carbon impact of local materials. We see the link of benefits in building operation of solar gain control methods and their impact on the embodied energy of a structure as a next step. Methodologies and toolsets for comparison must be established to aid the decision-making process. Furthermore, as suggested by the large member sizes of the proposed timber structures we see the opportunity for exploring multi-material solutions.

This project is a case study exploring a new design paradigm derived from the co-designing of a structurally integrated and solar optimized envelope for architectural construction. We established a workflow that can be adapted to variety of designs and different materials, site, and environmental constraints. Furthermore, we can show how carbon savings over a reference case can be used as a decision-making tool to inform materialization and design.

The disjointed architectural, energetic, and structural considerations of large parts of today's architectural and engineering practice can have significant detrimental effects on the sustainability of a project in terms of both embodied and operational carbon. It is vital for the disciplines to create new modes of thinking around sustainable construction, using energy and material efficiency as design drivers and to creating workflows that enable designers to include these considerations into early stages of design. We can show how architectural experimentation and expression are not in a direct conflict with sustainable building design but can indeed enable highly efficient structures. To address the global climate challenge, we must develop future architectural solutions that are optimal in an energetic sense, but also create flexible and high-quality spaces for their inhabitants.

In its pathway to net zero buildings, the International Energy Agency (IEA) calls for the reduction of material usage to save embodied carbon by 50% in order to reach the climate goals (Bouckaert et al. 2021). We see this call for action as an invitation to architects and engineers to collaborate and create innovative structures that serve the environment, built and otherwise.

# 8. Acknowledgment

This research was primarily sponsored by the Sustainable Design Lab and the Digital Structures group at MIT.

# 9. References

Aksamija, Ajla. 2015. "High-Performance Building Envelopes : Design Methods for Energy Efficient Facades." *Advances in Building Energy Research* 10 (2): 240–62.

American Institute of Steel Construction. 2021. "Environmental Product Declaration - Fabricated Hot-Rolled Structural Sections." https://www.aisc.org/globalassets/why-steel/epd-aisc-hr-sections-2021.pdf.

Anderson, Jane, and Alice Moncaster. 2020. "Embodied Carbon of Concrete in Buildings, Part 1: Analysis of Published EPD." *Buildings and Cities* 1 (1): 198–217. https://doi.org/10.5334/bc.59.

Arge, Kirsten. 2005. "Adaptable Office Buildings: Theory and Practice." *Facilities* 23 (3–4): 119–27. https://doi.org/10.1108/02632770510578494.

Asl, Mohammad Rahmani, Michael Bergin, AdamMenter, and Wei Yan. 2014. "BIM-Based Parametric Building Energy Performance MultiObjective Optimization." *32nd ECAADe Conference* 224: 10. http://autodeskresearch.com/pdf/bimparametric.pdf.

Assem, E. O., and A. A. Al-Mumin. 2010. "Code Compliance of Fully Glazed Tall Office Buildings in Hot Climate." *Energy and Buildings* 42 (7): 1100–1105. https://doi.org/10.1016/j.enbuild.2010.02.001.

Baudrillard, Jean. 1982. "The Beaubourg-Effect: Implosion and Deterrence." Atlas of Places. 1982. https://www.atlasofplaces.com/architecture/centre-pompidou/.

Bechthold, Martin, Jonathan King, Anthony Kane, Jeffrey Niemasz, and Christoph Reinhart. 2011. "Integrated Environmental Design and Robotic Fabrication Workflow for Ceramic Shading Systems." *Proceedings of the 28th International Symposium on Automation and Robotics in Construction, ISARC 2011*, 70–75. https://doi.org/10.22260/isarc2011/0010.

Bernett, Allison, Katharina Kral, and Timur Dogan. 2021. "Sustainability Evaluation for Early Design (SEED) Framework for Energy Use, Embodied Carbon, Cost, and Daylighting Assessment." *Journal of Building*

*Performance Simulation* 14 (2): 95–115. https://doi.org/10.1080/19401493.2020.1865459.

Bouckaert, Stéphanie, Araceli Fernandez Pales, Christophe McGlade, Uwe Remme, and Brent Wanner. 2021. "Net Zero by 2050 - A Roadmap for the Global Energy Sector." Paris. iea.li/nzeroadmap.

Brown, Nathan, Stavros Tseranidis, and Caitlin Mueller. 2015. "Multi-Objective Optimization for Diversity and Performance in Conceptual Structural Design." *Proceedings of the International Association for Shell and Spatial Structures (IASS) Symposium "Future Visions,"* no. 20: 1–12. http://digitalstructures.mit.edu/files/2015-09/ncb-iass-paper-final.pdf.

Buelow, Peter Von. 2014. "ParaGen : Performative Exploration of Generative Systems," no. May.

Building Transparency. 2021. "EC3." 2021. https://buildingtransparency.org/ec3/.

Crawley, D. B., C. O. Pedersen, L. K. Lawrie, and F. C. Winkelmann. 2000. "Energy plus: Energy Simulation Program." *ASHRAE Journal* 42 (4): 49–56.

Ekici, Berk, Z. Tuğçe Kazanasmaz, Michela Turrin, M. Fatih Taşgetiren, and I. Sevil Sariyildiz. 2021. "Multi-Zone Optimisation of High-Rise Buildings Using Artificial Intelligence for Sustainable Metropolises. Part 1: Background, Methodology, Setup, and Machine Learning Results." *Solar Energy* 224 (October 2020): 373–89. https://doi.org/10.1016/j.solener.2021.05.083.

Evins, Ralph. 2013. "A Review of Computational Optimisation Methods Applied to Sustainable Building Design." *Renewable and Sustainable Energy Reviews* 22: 230–45. https://doi.org/10.1016/j.rser.2013.02.004.

Fan, Zhaoxiang, Mengxuan Liu, and Shuoning Tang. 2022. "A Multi-Objective Optimization Design Method for Gymnasium Facade Shading Ratio Integrating Energy Load and Daylight Comfort." *Building and Environment* 207 (6): 108527. https://doi.org/10.1016/j.buildenv.2021.108527.

Foraboschi, Paolo, Mattia Mercanzin, and Dario Trabucco. 2014. "Sustainable Structural Design of Tall Buildings Based on Embodied Energy." *Energy and Buildings* 68 (PARTA): 254–69. https://doi.org/10.1016/j.enbuild.2013.09.003.

Foster + Partners. 1986. "Hongkong and Shanghai Bank Headquarters." 1986. https://www.fosterandpartners.com/projects/hongkong-and-shanghai-bank-headquarters/.

Gan, Vincent J.L., C. M. Chan, K. T. Tse, Irene M.C. Lo, and Jack C.P. Cheng. 2017. "A Comparative Analysis of Embodied Carbon in High-Rise Buildings Regarding Different Design Parameters." *Journal of Cleaner Production* 161: 663–75. https://doi.org/10.1016/j.jclepro.2017.05.156.

Gao, Hao, Christian Koch, and Yupeng Wu. 2019. "Building Information Modelling Based Building Energy Modelling: A Review." *Applied Energy* 238 (January): 320–43. https://doi.org/10.1016/j.apenergy.2019.01.032.

Häkkinen, Tarja, Matti Kuittinen, Antti Ruuska, and Nusrat Jung. 2015. "Reducing Embodied Carbon during the Design Process of Buildings." *Journal of Building Engineering* 4: 1–13. https://doi.org/10.1016/j.jobe.2015.06.005.

Hamel, Scott, and Kara Peterman. 2019. "Thermal Breaks in Building Envelopes, Recent Research Findings." *Structuremag*, January 2019. https://www.structuremag.org/wp-content/uploads/2018/12/261901-D-StructuralSustainability-Hamel.pdf.

Hart, Jim, Bernardino D'Amico, and Francesco Pomponi. 2021. "Whole-Life Embodied Carbon in Multistory Buildings: Steel, Concrete and Timber Structures." *Journal of Industrial Ecology* 25 (2): 403–18. https://doi.org/10.1111/jiec.13139.

Herzog, Thomas, Roland Krippner, and Werner Lang. 2004. *Facade Construction Manual*. *Facade Construction Manual*. https://doi.org/10.11129/detail.9783034614566.

Jayaweera, Nadeeka, Upendra Rajapaksha, and Inoka Manthilake. 2021. “A Parametric Approach to Optimize Solar Access for Energy Efficiency in High-Rise Residential Buildings in Dense Urban Tropics.” *Solar Energy* 220 (February): 187–203. https://doi.org/10.1016/j.solener.2021.02.054.

Jiang, Caigui, Jun Wang, Philippe Bompas, Helmut Pottmann, and Johannes Wallner. 2013. “Freeform Shading and Lighting Systems from Planar Quads.” *Rethinking Prototyping*, 335–46.

Jones, Craig, and Geoffrey Hammond. 2019. “Inventory of Carbon and Energy (ICE) Database.” 2019. https://circularecology.com/embodied-carbon-footprint-database.html.

Konis, Kyle, Alejandro Gamas, and Karen Kensek. 2016. “Passive Performance and Building Form: An Optimization Framework for Early-Stage Design Support.” *Solar Energy* 125: 161–79. https://doi.org/10.1016/j.solener.2015.12.020.

Lee, Adam D., Paul Shepherd, Mark C. Evernden, and David Metcalfe. 2018. “Optimizing the Architectural Layouts and Technical Specifications of Curtain Walls to Minimize Use of Aluminium.” *Structures* 13: 8–25. https://doi.org/10.1016/j.istruc.2017.10.004.

Liu, Chengqing, Qinfeng Li, Zheng Lu, and Handan Wu. 2018. “A Review of the Diagrid Structural System for Tall Buildings.” *Structural Design of Tall and Special Buildings* 27 (4): 1–10. https://doi.org/10.1002/tal.1445.

Manzan, Marco. 2014. “Genetic Optimization of External Fixed Shading Devices.” *Energy & Buildings* 72: 431–40. https://doi.org/10.1016/j.enbuild.2014.01.007.

Mardaljevic, John. 2003. “PRECISION MODELLING OF PARAMETRICALLY DEFINED SOLAR SHADING SYSTEMS : PSEUDO-CHANGI.” In *Building Simulation 2003*, 823–30. Eindhoven, Netherlands: Eighth International IBPSA Conference. http://www.ibpsa.org/proceedings/BS2003/BS03_0823_830.pdf.

Marsh, Andrew. 2003. “Computer-Optimized Shading Design.” In *International, Eighth Conference, Ibpsa*, 831–38.

Mcglashan, Niko, Curtis Ho, Simon Breslav, David Gerber, and Azam Khan. 2021. “Sustainability Certification Systems as Goals in a Generative Design System,” no. June: 15–17.

Méndez, Tomás, Alfonso Capozzoli, Ylenia Cascone, and Mario Sassone. 2015. “The Early Design Stage of a Building Envelope : Multi-Objective Search through Heating , Cooling and Lighting Energy Performance Analysis” 154: 577–91. https://doi.org/10.1016/j.apenergy.2015.04.090.

Minaei, Mahsa, and Ajla Aksamija. 2020. “Performance-Based Facade Framework Automated and Multi-Objective Simulation and Optimization,” 485–92.

Moncaster, A. M., and J-Y. Song. 2012. “A Comparative Review of Existing Data and Methodologies for Calculating Embodied Energy and Carbon of Buildings.” *International Journal of Sustainable Building Technology and Urban Development* 3 (1): 26–36. https://doi.org/10.1080/2093761X.2012.673915.

Moon, Kyoung Sun, Jerome J. Connor, and John E. Fernandez. 2007. “Diagrid Structural Systems for Tall Buildings: Characteristics and Methodology for Preliminary Design.” *Structural Design of Tall and Special Buildings* 16 (2): 205–30. https://doi.org/10.1002/tal.311.

Mueller, Caitlin T., and John A. Ochsendorf. 2015. “Combining Structural Performance and Designer Preferences in Evolutionary Design Space Exploration.” *Automation in Construction* 52: 70–82. https://doi.org/10.1016/j.autcon.2015.02.011.

Omidfar, Azadeh. 2011. “Design Optimization of a Contemporary High Performance Shading Screen-Integration of ‘form’ and Simulation Tools.” *Proceedings of Building Simulation 2011: 12th Conference of International Building Performance Simulation Association*, no. January 2011: 2491–98.

Oswald, Adam. 2021. “Evolutionary Computing in a Performative Facade Design Process.” In *SimAUD*.

http://simaud.org/2021/content.php?f=71.pdf.

Peters, Terri, Jake Wolf, Brady Peters, and Ted Kesik. 2019. “Generative Design Approaches to Daylight in MURBs.” *Building Simulation Conference Proceedings* 2 (September): 1247–54. https://doi.org/10.26868/25222708.2019.211380.

Preisinger, Clemens, and Moritz Heimrath. 2014. “Karamba - A Toolkit for Parametric Structural Design.” *Structural Engineering International: Journal of the International Association for Bridge and Structural Engineering (IABSE)* 24 (2): 217–21. https://doi.org/10.2749/101686614X13830790993483.

Sargent, Jon A., Jeffrey Niemasz, and Christoph F. Reinhart. 2011. “SHADERADE: Combining Rhinoceros and Energyplus for the Design of Static Exterior Shading Devices.” *Proceedings of Building Simulation 2011: 12th Conference of International Building Performance Simulation Association*, 310–17.

Schittich, Christian, Steffi Lenzen, Sophie Karst, Michaela Linder, and Eva Schönbrunner, eds. 2013. *Best of Detail: Büro/Office*. DE GRUYTER. https://doi.org/10.11129/detail.9783955531140.

Schlueter, Arno, and Frank Thesseling. 2009. “Building Information Model Based Energy/Exergy Performance Assessment in Early Design Stages.” *Automation in Construction* 18 (2): 153–63. https://doi.org/10.1016/j.autcon.2008.07.003.

Schweber, Libby, and Hasan Haroglu. 2014. “Comparing the Fit between BREEAM Assessment and Design Processes.” *Building Research and Information* 42 (3): 300–317. https://doi.org/10.1080/09613218.2014.889490.

Shi, Zhongming, Jimeno A. Fonseca, and Arno Schlueter. 2021. “A Parametric Method Using Vernacular Urban Block Typologies for Investigating Interactions between Solar Energy Use and Urban Design.” *Renewable Energy* 165: 823–41. https://doi.org/10.1016/j.renene.2020.10.067.

Solemma. 2021. “Climate Studio.” 2021.

Tang, Ming, and Mark Landis. 2021. “Fixed Shading Device Design with the Performance-Based- Design and Energy Simulation.” In *SimAUD*.

Taubenböck, H., H. Debray, C. Qiu, M. Schmitt, Y. Wang, and X. X. Zhu. 2020. “Seven City Types Representing Morphologic Configurations of Cities across the Globe.” *Cities* 105 (May): 102814. https://doi.org/10.1016/j.cities.2020.102814.

Trabucco, Dario. 2016. “End of Life of a Tall Building.” In *Tall Buildings a Strategic Design Guide*, edited by N. Clark and B. Price, 123–129. Newcastle upon Tyne: RIBA Publishing.

Trabucco, Dario, and Martina Belmonte. 2021. “Tall Buildings And Life Cycle Approaches : A Debate That Must Be Started.” *CTBUH Journal* |, no. III: 44–50. https://global.ctbuh.org/resources/papers/download/4491-tall-buildings-and-life-cycle-approaches-a-debate-that-must-be-started.pdf.

Turrin, Michela, Peter Von Buelow, Axel Kilian, and Rudi Stouffs. 2012. “Automation in Construction Performative Skins for Passive Climatic Comfort A Parametric Design Process.” *Automation in Construction* 22: 36–50. https://doi.org/10.1016/j.autcon.2011.08.001.

Ürge-Vorsatz, Diana, Ksenia Petrichenko, Miklos Antal, Maja Staniec, Michael Labelle, Eren Ozden, and Elena Labzina. 2012. *Best Practice Policies for Low Energy and Carbon Buildings: A Scenario Analysis*. http://www.gbpn.org/sites/default/files/08.CEU Technical Report copy_0.pdf.

Vancura, Peter. 2014. “An Exoskeleton with a TWIST.” *Modern STEEL CONSTRUCTION*, 2014. https://www.aisc.org/globalassets/modern-steel/archives/2014/10/exoskeleton.pdf.

Wang, J., C. Jiang, P. Bompas, J. Wallner, and H. Pottmann. 2013. “Discrete Line Congruences for Shading and Lighting Discrete Line Congruences for Shading and Lighting.” In *Eurographics Symposium on Geometry Processing*. https://doi.org/10.1111/cgf.12172.

Ward, G. and Shakespeare, R. 1998. *Rendering with Radiance: The Art and Science of Lighting Visualization*. *Morgan Kaufman*.

Westermann, Paul, and Ralph Evins. 2019. "Surrogate Modelling for Sustainable Building Design – A Review." *Energy and Buildings* 198: 170–86. https://doi.org/10.1016/j.enbuild.2019.05.057.

World Green Building Council (WGBC), IEA, and UN-Environment. 2018. "2018 Global Status Report." https://webstore.iea.org/download/direct/2408?fileName=2018_Global_Status_Report.pdf.

Wörsdörfer, Mechthild, Timur Gül, John Dulac, Thibaut Abergel, Chiara Delmastro, Peter Janoska, Kevin Lane, and Andrew Prag. 2019. "Perspectives for the Clean Energy Transition – The Critical Role of Buildings." Paris. www.iea.org.

Wortmann, Thomas, and Thomas Fischer. 2020. "Does Architectural Design Optimization Require Multiple Objectives? A Critical Analysis." *RE: Anthropocene, Design in the Age of Humans - Proceedings of the 25th International Conference on Computer-Aided Architectural Design Research in Asia, CAADRIA 2020* 1: 365–74.

Zaha Hadid Architects. 2018. "Morpheus Hotel at City of Dreams, Macau." 2018. https://www.zaha-hadid.com/architecture/city-of-dreams-hotel-tower-cotai-macau/.

———. 2020. "One Thousand Museum." 2020. https://www.zaha-hadid.com/design/1000-museum/.

Zargar, Seyed Hossein, and Nathan C. Brown. 2021. "Deep Learning in Early-Stage Structural Performance Prediction." *Proceedings of the International Association of Shell and Spatial Structures 2020/2021 (in Press)*, no. December.

Zhao, Jing, and Yahui Du. 2020. "Multi-Objective Optimization Design for Windows and Shading Configuration Considering Energy Consumption and Thermal Comfort: A Case Study for Office Building in Different Climatic Regions of China." *Solar Energy* 206 (August): 997–1017. https://doi.org/10.1016/j.solener.2020.05.090.